Assessment of the skin barrier function in the reconstructed human epidermis using a multimodal approach at molecular, tissue and functional levels

Joudi Bakar, Rime Michael-Jubeli, Rindala El Khoury, Sabrina Hamla, Ali Assi, Arlette Baillet-Guffroy, Ali Tfayli

▶ **To cite this version:**

Joudi Bakar, Rime Michael-Jubeli, Rindala El Khoury, Sabrina Hamla, Ali Assi, et al.. Assessment of the skin barrier function in the reconstructed human epidermis using a multimodal approach at molecular, tissue and functional levels. Analyst, 2021, 146 (14), pp.4649-4658. 10.1039/D1AN00465D . hal-04528245

HAL Id: hal-04528245
https://hal.science/hal-04528245

Submitted on 2 Apr 2024

HAL is a multi-disciplinary open access archive for the deposit and dissemination of scientific research documents, whether they are published or not. The documents may come from teaching and research institutions in France or abroad, or from public or private research centers.

L'archive ouverte pluridisciplinaire **HAL**, est destinée au dépôt et à la diffusion de documents scientifiques de niveau recherche, publiés ou non, émanant des établissements d'enseignement et de recherche français ou étrangers, des laboratoires publics ou privés.

Assessment of the Skin Barrier Function in the Reconstructed Human Epidermis using a Multimodal Approach at molecular, tissue and functional levels.

Joudi Bakar, Rime Michael-Jubeli *, Rindala El Khoury, Sabrina Hamla, Ali Assi, Arlette Baillet-Guffroy, Ali Tfayli. Lipides : systèmes analytiques et biologiques, Université Paris-Saclay, 92296, Châtenay-Malabry, France.

Author(s):

1- Joudi Bakar : joudi.bakar@u-psud.fr, Lipides : systèmes analytiques et biologiques, Université Paris-Saclay, 92296, Châtenay-Malabry, France.

2- Rime Michael-Jubeli : **This author accept correspondance and proofs**, rime.michael-jubeli@u-psud.fr, Lipides : systèmes analytiques et biologiques, Université Paris-Saclay, 92296, Châtenay-Malabry, France. Orcid ID : 0000-0002-2944-5295.

3- Rindala El Khoury : contact.rindala@gmail.com, Lipides : systèmes analytiques et biologiques, Université Paris-Saclay, 92296, Châtenay-Malabry, France.

4- Sabrina Hamla : hamla.sab@gmail.com, Lipides : systèmes analytiques et biologiques, Université Paris-Saclay, 92296, Châtenay-Malabry, France.

5- Ali Assi: ali.assi@u-psud.fr, Lipides : systèmes analytiques et biologiques, Université Paris-Saclay, , 92296, Châtenay-Malabry, France.

6- Arlette Baillet-Guffroy: arlette.baillet-guffroy@u-psud.fr, Lipides : systèmes analytiques et biologiques, Université Paris-Saclay, 92296, Châtenay-Malabry, France.

7- Ali Tfayli : ali.tfayli@u-psud.fr, Lipides : systèmes analytiques et biologiques, Université Paris-Saclay, , 92296, Châtenay-Malabry, France.

***Corresponding author**: Rime Michael-Jubeli, 5 rue Jean-Baptiste Clément - 92290 Châtenay-Malabry – France, +33146835904, fax: +33146835458, rime.michael-jubeli@u-psud.fr

Abbreviations:

1-O-E(EO)Cer : double esterified ceramide: on the 1-O-position of sphingoid base with long to very long chain acyl residues (1-O-E) and on the position of ω-hydroxyl group of fatty acid with the linoleic acid (EO).

Ads: α-hydroxy DihydroSphingosine

AH: α-hydroxy 6-Hydroxysphingosine

AP: α-hydroxy Phytosphingosine

AS: α-hydroxy Sphingosine

APPI: Atmospheric Pressure PhotoIonization

CER: Ceramide

CLS: Classical Least Squares

D: Differentiation Day

EAH: Esterified α-hydroxy 6-Hydroxysphingosine

EAP: Esterified α-hydroxy Phytosphingosine

ENH: Esterified Non-hydroxy 6-Hydroxysphingosine

ENT: Esterified/Non-hydroxy/T: dihydroxy-dihydro sphingosine

EOH: Esterified ω-hydroxy 6-Hydroxysphingosine

EOS: Esterified ω-hydroxy Sphingosine

GlcCER: GlucosylCeramide

HPLC: High-Performance Liquid Chromatography

HR-MS^n : High-Resolution Mass Spectrometry

NDS: Non-hydroxy DihydroSphingosine

NP: Non-hydroxy Phytosphingosine

NPLC: Normal-Phase Liquid Chromatography

NS: Non-hydroxy Sphingosine

NT: Non-hydroxy/T: dihydroxy-dihydro sphingosine

RHE: Reconstructed Human Epidermis

RSD: Relative Standard Deviation

RT: Retention Time

SC: *Stratum Corneum*

SG: *Stratum Granulosum*

SM: Sphingomyelin

UV: Ultraviolet

VLC: Very Long Chain

ULC: Ultra Long Chain

Abstract

Reconstructed human epidermis models are used as epidermis alternatives in skin researches. It is necessary to provide molecular and functional characterization in order to assess these models. Our aim is to make a link between the barrier function and the structure and the composition of the *Stratum Corneum* using several complementary techniques. Three studies were used on Reconstructed Human Epidermis during the keratinocyte differentiation process: i- caffeine percutaneous penetration kinetic. ii- epidermis thickness measurement, *Stratum Corneum* formation and lipids organization by Raman microspectroscopy. iii- lipid composition evolution by liquid chromatography coupled to high resolution mass spectrometry. Results demonstrated that the caffeine penetration decreased along the differentiation process. Raman in depth images demonstrated an increase in *Stratum Corneum* and RHE thickness accompanied with an evolution of lipid organization. Lipid analysis showed an increase of ceramide amount and an inverse relationship between ceramide and their precursor's levels during the differentiation process. A different behavior between several ceramides subclasses is highlighted and relied to corresponding differentiation stage. The generation of the most important ceramides for the barrier function is closely followed. A period shift between lipids generation and their organization was found. Our analytical data allowed identifying 3 groups of maturation days: before day 15, between day 15 and 19, and after day 19. The chemical and physiological states of the barrier function for each group are described thanks to the multimodal approach.

Keywords: Reconstructed Human Epidermis, barrier function, keratinocyte differentiation, multimodal approach, Raman microspectroscopy, NPLC/HR-MS^n.

Introduction

Reconstructed human skin epidermis (RHE) is the first tissue generated *in vitro* that mimics its native counterpart to a high degree [2]. It is a three-dimensional model of normal human–derived epidermal keratinocytes that consists of a viable epidermis, including organized basal, spinous and granular layers as well as an underlying multilayered stratum corneum (*SC*). It is essentially used in the cosmetic *in vitro* testing such as the evaluation of the irritation or the penetration of an active ingredient. The *in vitro* reconstructed skin models pre-require a barrier function of the *SC* layer similar to that of the native skin. For this purpose, various techniques were used to characterize the RHE models and to assess the barrier permeability: A/ Morphological studies of tissue structure using light and electron microscopies [3] B/ Lipid organization studies using the X-ray diffraction and freeze fracture electron microscopic techniques [3-5]. C/ RHE lipid profile analysis using separation methods such as thin-layer liquid and gas chromatography [3, 6, 7]. D/ Percutaneous penetration studies with typically caffeine as a reference molecule [8] using high Performance Liquid Chromatography (HPLC)[9, 10] , IR absorption or Raman scattering[11, 12]. In the studies cited above, only one technique at a time is used to evaluate the skin barrier function. Thus, the results obtained provide information concerning a single aspect of the skin barrier, while the barrier function is the result of a complex biological process that encompasses functional, structural and morphological aspects. In this order, and to better asses the RHE barrier development and maturation, the present study is focused on combining three complementary analytical methods:

- HPLC-UV study: Allows for the assessing of the establishment of the skin barrier function by following the caffeine percutaneous penetration kinetics.

- Raman microspectroscopy study: Allows for the assessing of the *SC* evolution, lipid conformation and epidermis thickness. This technique allows a non-invasive diagnostic and a powerful characterization of lipid conformation and organization. It allows a free staining observation of epidermal cells as well as a tissue or cell culture, in contrast to the light and electron microscopies in which the tissue should be stained before analysis [13].

- High Performance Liquid Chromatography coupled to High Resolution Mass Spectrometry HPLC/HR-MS^n: allows assessing the evolution of the lipid biomarkers (the glucosylceramides (GlcCER), the sphingomyelins (SM), the ceramides and the ceramides' subclasses).

It is the combination of the three approaches that allowed us to determine, for the first time in the literature, the RHE differentiation period were the skin barrier becomes functional.

Materials and methods

The chemicals

Solvents for extraction and for normal phase liquid chromatography coupled to high resolution mass spectrometry (NPLC/HR-MS^n) were of HPLC grade, caffeine and the internal standard (1-Eicosanol) and were all purchased from Sigma-Aldrich (Saint Quentin Fallavier, France).

The skin samples

Reconstructed Human Epidermis models (RHE) "Episkin® (Episkin, France)", is a three dimensional model of normal human–derived epidermal keratinocytes. It consists of organized basal, spinous and granular layers, and a multilayered *stratum corneum* (*SC*). The differentiation process takes around two weeks, which allows for the development of stratified layers [14]. A triplicate of 10 (RHE) samples whose batch number is (16 RHE-040), was received from D12 of keratinocyte maturation. On delivery, samples were immersed in a maintenance medium and incubated for 10 days, in order to reach the D24 of the differentiation process. A duplicate set of RHE was used for a caffeine penetration study and then for lipid analysis studies via LC/HR-MS^n. The third set was then used for Raman microspectroscopy analysis.

The kinetic of caffeine percutaneous penetration

200µL of caffeine solution (2.1 mg/mL in PBS) were deposited at the surface of each RHE sample after different maturation days of keratinocytes (D12, D13, D14, D15, D17, D18, D19, D20, D22 and D24). Following the caffeine application, 300 µL of liquid were taken from the receptor fluid on the other side of each sample after 2, 3, 4, 6, and 8 hours. At each interval, the 300 µL of liquid volume collected from each RHE sample was replaced by 300 µL of maintenance medium.

The measurements of the caffeine concentration that passed through the RHE samples were recorded using a high-performance liquid chromatography, with an external calibration and a 7 concentration range (from 0.202µg/mL to 404 µg/mL). The separation was carried out on a C18 Kromasil column measuring 150 mm x 4.6 mm, Ø 5µm, at 35

°C. The Kontron Instruments 465 C4 INJ 003 Auto Sampler Injector was used to inject a volume of 20µL. The solvents were continuously degassed by the Kontron Instruments 422 C4 PMV 004 pump. The mobile phase was composed of water / methanol / acetic acid (75: 25: 1 v / v), with a flow rate of 1mL/min. The HPLC system was coupled with the Kontron Instruments 335 C4 DUV 003 UV spectrophotometric detector. The detection was recorded at a wavelength of 273 nm. The chromatographic data was exploited by the Kroma 2000 system. The analysis time for each injection was 10 minutes (since the retention time of the caffeine peak is 6 minutes).

To estimate the caffeine concentration, a calibration range of reference solutions was prepared daily and analyzed before testing the samples. Calibration curves were then calculated, relating the area under curve of caffeine peak to that of the known concentration, [area under curve = f (concentration)]. All calibration ranges (obtained from reference solutions) gave a regression coefficient $R^2 > 0.999$. The inter-range variability was evaluated by calculating the relative standard deviation (RSD) of the slopes. RSD was found to be lower than 5%.

The extraction of lipids

A duplicate of RHE samples of each maturation day (D12, D13, D14, D15, D17, D18, D19, D20, D22 and D24) was used in this study. The total lipid of the RHE samples were extracted by the modified method of Bligh and Dyer [15]. The epidermis was then separated from the nitrocellulose support using pliers and placed into 1.5mL of MeOH and vortexed for 2 min. Then, 3mL of chloroform containing Eicosanol as an internal standard (0.3 mg/mL on chloroform) was added. The mixture was finally incubated for 1 hour at room temperature in the dark. The separation phase was induced by the addition of 1.5mL of water using a magnetic agitator for 10 minutes at room temperature. For better separation of the two phases, a centrifugation step at 3000 rpm for 10 minutes at 20° C was done. The chloroform phase was collected and the aqueous phase, which contains (H_2O + methanol + skin), was washed with 2 mL of chloroform. Then the whole mixture was vortexed and centrifuged for 10 minutes at 3000 rpm and at 20 ° C. This step was repeated twice. The organic phases were collected and evaporated under a stream of nitrogen until reaching dryness. The lipid residue was taken up with 100 µL of chloroform [1].

The Raman spectrometer instrumentation: The thickness of the Reconstructed Human Epidermis and the evolution of the lipid biomarkers

Raman spectral acquisition and spectral imaging were performed with the use of a LabRam HR evolution (Horiba scientific, Palaiseau, France). A 632.8 nm He-Ne laser with 10 mW power and a long focal distance microscope objective MPLFLN 100X (0.90 NA, Olympus) were used. The Confocal pinhole was set to 200 µm. The collected light was filtered through an edge filter and dispersed with a 4 cm^{-1} spectral resolution, using a grating of 300 grooves/mm over a wavenumber range of 400-3800 cm^{-1}. Spectral acquisition pre-processing and processing were performed using Labspec 6.1.9 software (Horiba Scientific, Villeneuve d'Ascq, France). For each spectrum, a 5 s exposure time was used with 5 accumulations.

In-depth Raman Imaging: For Raman imaging, RHE samples were deposited on CaF_2 slides. Optical cross sections (XZ confocal maps) were obtained in a point-by-point mode perpendicular to the dry RHE surface. A Raman spectrum was produced every 2 µm from -10 µm (before the *SC* surface) to +25 µm (under the skin surface) with a 2 µm step-size (objective displacement). All spectra were subjected to the same preprocessing protocol. The spectra were smoothed using the Savitsky-Golay algorithm, using 5 points and the baseline correction was done by a 3-order polynomial function.

Raman Data Processing

Epidermis thickness calculation: For each maturation day, 6 profiles representing 6 different locations of the surface were obtained from the confocal maps. The spectral profiles were obtained from the area under curve (AUC) of the band 1004 cm^{-1}. The latter is specific to phenylalanine. When the collection focus is outside the surface of the sample, the signal is near to zero. When the moving down, the spectra collected presented higher AUC values. In this manner, the positions of the outer and lower surfaces of the RHE are considered at the outer and inner mid height of the maximum. The distance between both positions gives the thickness of RHE measured by Raman spectroscopy (figure 1) [16].

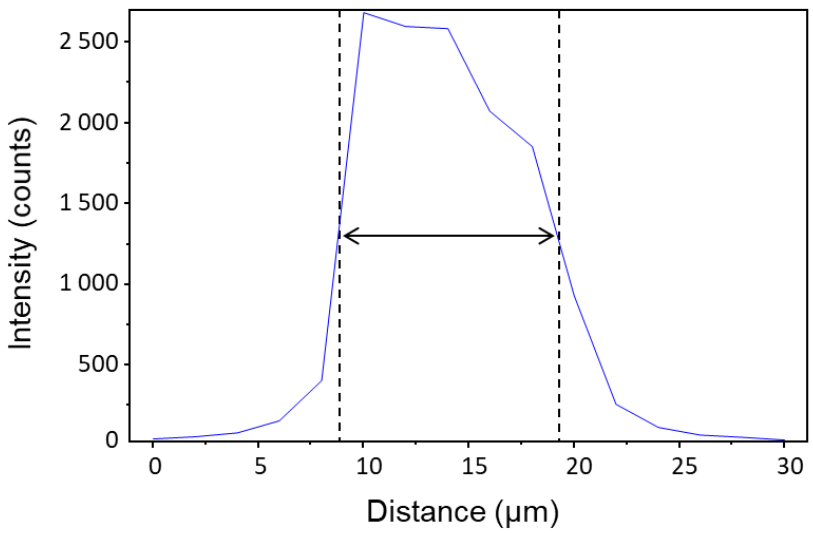

Figure 1 *The spectral profile represents the method of the epidermis thickness calculation for each maturation day*

Classical least squares fitting (CLS) for the evaluation of stratum corneum evolution: In order to follow the evolution of *Stratum Corneum* formation during the maturation days, reference spectra were collected from human skin cross sections. Spectra were collected from *Stratum Corneum* (*SC*) while viable epidermis and average spectra were calculated and used as reference (supplementary data 1).

For each pixel of the confocal Raman maps, the spectrum was de-convoluted with the use of the Labspec 6.1.9 software (Horiba Scientific, Villeneuve d'Ascq, France) by introducing the different contributions of CLS fitting. As a result, a spectral contribution was obtained for both *SC* and viable epidermis in each pixel of the image. The pseudo-color maps can thus highlight the contribution of both parts of RHE (figure 4).

For all the fits, the fit error was less than 0.7 %. It should be noted that only a spectral contribution percentage is obtained and not a mass or molar ratio. The spectral contribution of SC reference spectrum is thus obtained for all the pixels in the spectral maps. This enabled to calculate a mean percentage of *SC* contribution at each day of maturation.

Lipid conformational order: The ratio of $\nu_{asym}CH_2$ (2882 cm^{-1})/$\nu_{sym}CH_2$ (2852 cm^{-1}) was studied. This ratio is generally used as an indicator of the conformational state and the lateral packing (Figure 5). High values are associated with a compact state in the lipid packing, while a decrease is indicative of a loosening [17].

The analysis of the biomarkers: instrumentation and analytical method NP-LC/HR-MS^n

The analysis of the extracted lipid was done by HPLC (Dionex Ultimate 3000, ThermoFisher Scientific, San Jose, CA). Separation of lipid occurred in NPLC using (PVA)-Sil column (PVA-bonded column; 5 µm particle size, 150 × 4.6 mm) purchased from YMC (Kyoto, Japan). A solvent gradient of Heptane/ethyl acetate (99.8: 0.2 v/v) (Solvent A), acetone and ethyl acetate (2: 1 v/v) with acetic acid (0.02% v/v) (Solvent B) and 2-propanol/ water (85:15v/v) (with acetic acid and ethanolamine each at 0.025% v/v) (solvent C) was used. A flow rate of 1 mL/min was done. The injected volume was 10 µL. Detection was performed using two detectors simultaneously: a Corona CAD® and a hybrid mass spectrometer LTQ-Orbitrap Velos Pro (Thermo Fisher Scientific, San Jose, CA) equipped with an Atmospheric Pressure Photoionization (APPI) source. APPI positive ion mode was used to analysis the extracted lipid. The mass scan range was 220-1800 atomic mass units (amu). A full scan detection mode and fragmentation was performed by the orbital trap at a resolution of 100, 000. The analytical conditions are detailed in a previous work [1].

Results

As previously commented, in our study we aim to evaluate the maturation day of keratinocytes while cross-linking different parameters together: 1- the kinetic of caffeine percutaneous penetration, 2- the RHE thickness, 3- the evolution of the *SC* contribution in RHE, 4- the lipids' conformational state, 5- the evolution of lipids composition and 6- the evolution of the ceramides' subclasses.

The kinetic of caffeine percutaneous penetration

Figure 2 shows the kinetic of caffeine percutaneous penetration over an 8 hour duration at each maturation day of the keratinocytes. For a defined maturation day, the penetration of caffeine increased with time. This is a normal behavior already described in literature [8]. However, for a defined application time, the penetration decreased along maturation days: during advanced maturation, the caffeine penetrated less. In order to take into account the global penetration profiles and not at a specific point in time, the slopes of the penetration linear regressions obtained for each maturation day were considered. With regards to the slopes (supplementary data 2, table 1, column 2), we detected a decrease of slope values with the evolution of the cell differentiation days. According to these results and as shown in figure 2, we can distinguish three separated groups: The first group concerns the slopes representing D12, 13 and 14. For these

maturation days, the caffeine amount that passed through the RHE samples was very high due to a not-so- fully formed *Stratum Corneum* and a non-established barrier function which permits a strong penetration of the molecules.

The second group regroups the slopes of D15, 17, 18 and 19. In this group we observed the decrease of the slope values *i.e.* the decrease of caffeine penetration in comparison with the first group.

Finally, from D20 to D24, a third group was identified. The caffeine quantity that passed through RHE samples was much lower.

At this stage of the study one can conclude on a direct relation between the maturation days and the decrease of the penetration of caffeine.

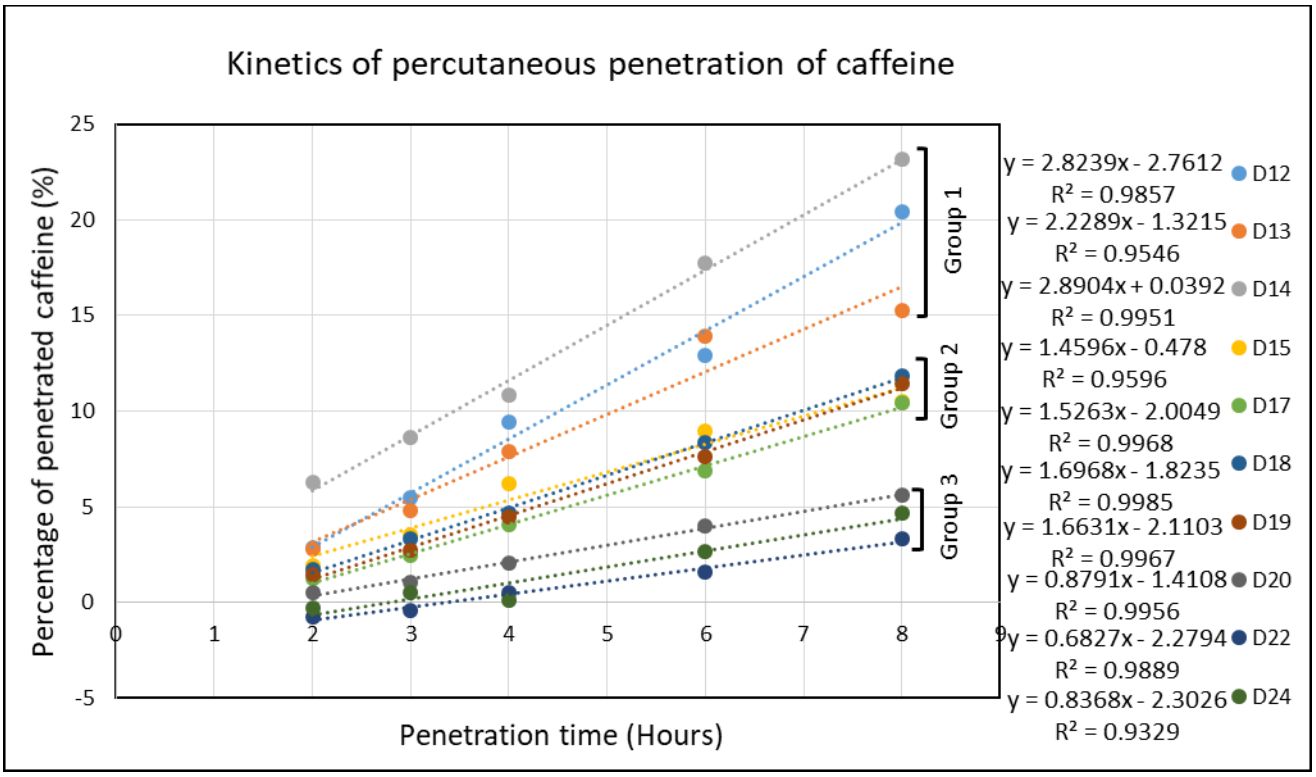

Figure 2 *The kinetic of caffeine percutaneous penetration through the Reconstructed Human Epidermis model (RHE). Three groups of penetration profiles are clearly identified. *D: maturation day*

The thickness of the Reconstructed Human Epidermis

Since caffeine percutaneous penetration might be linked to the thickness of the epidermis, the average values of RHE thickness were calculated (Supplementary data 2, table 1, column 4 and supplementary data 3). These results show a gradual increase of the RHE thickness along the maturation days, following a linear fit with a correlation coefficient $R^2 = 0.95$ (data not shown). Figure 3 shows the correlation between the caffeine percutaneous penetration kinetics' slopes and the epidermis thickness during the RHE maturation days. The caffeine percutaneous penetration decreases when the RHE thickness increases. Figure. 3 shows clearly the three groups of maturation days.

However, even if the global evolution of caffeine penetration is concordant with the RHE thickness, we can observe that in group 2, the thickness increase is not accompanied by a significant variation in the caffeine penetration profiles. We can conclude that the evolution of the skin barrier is not only related to the thickness of the RHE. This is the reason we decided to investigate further on the *SC*.

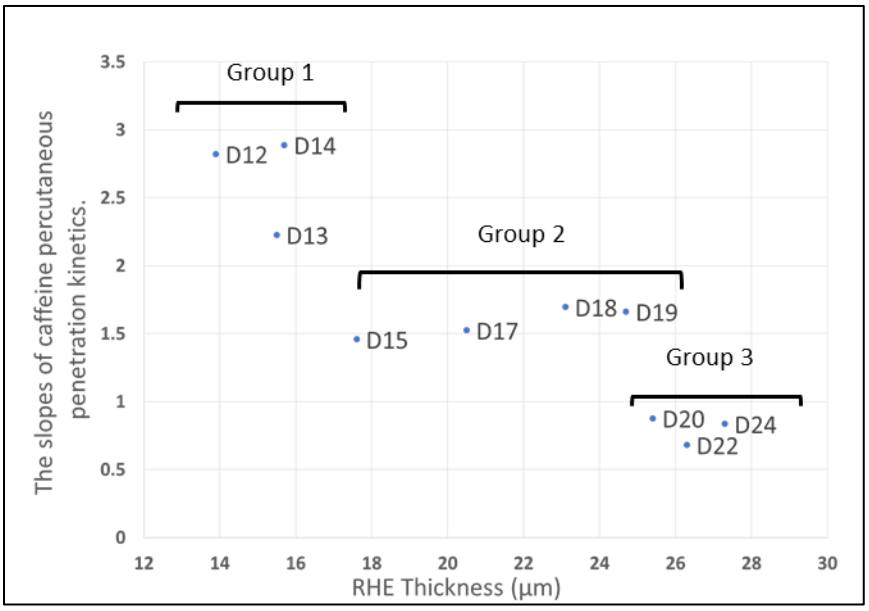

Figure 3 *The correlation between the caffeine percutaneous penetration kinetics slopes and the epidermis thickness during the RHE maturation days. Three separated groups of maturation were detected: D12 to D14, D15 to D19 and D20 to D24.*

The evolution of the *SC* contribution in RHE

The reduction of the penetration of caffeine may be due not only to the epidermis thickness, but also to the *SC* contribution. To confirm this hypothesis, the *SC* evolution and contribution were studied. Thus, CLS fitting based on reference spectra from human *SC* and *SG* was applied to the Raman spectra all in -depth RHE Raman maps for the different maturation days. Figure 4 demonstrates that the *SC* layer (red color) increased along the differentiation process. One can observe that the SC layer (red color) of the first three days D12, D13, and D14 is almost similar. After D15, the SC is more important. Days 20 and 22 appear to have the thickest layer of SC. These results can give us a first assessment of the SC evolution during RHE differentiation process.

As shown in figure 4 and in supplementary data 2 (table 1, column 5), the SC contribution was the lowest for D12 to D14. Between D15 and up to D18, a clear increase of *SC* contribution percentage is observed. Finally, from D19 and up to D24 the highest *SC* contribution percentage is detected. Despite the high SC contribution at D19, its related penetration kinetics is closer to the second group, this may be explained by a time shift between lipids formation and organization. These results are consistent with results on the conformational order of lipids shown in figure. 4. We can observe that day 20 has a better lateral packing.

Moreover, we can distinguish 3 groups: D12 and D14 where SC contribution percentage is the lowest. The second group regroups D15 and up to D18. In this group, there is a clear increase of *SC* contribution percentage compared to the first group. Finally, the group from D19 and up to D24 has the higher *SC* contribution percentage compared with the first two groups. These results are consistent with results of the epidermis thickness shown in figure. 3. We can observe that day 20 has the most important SC contribution.

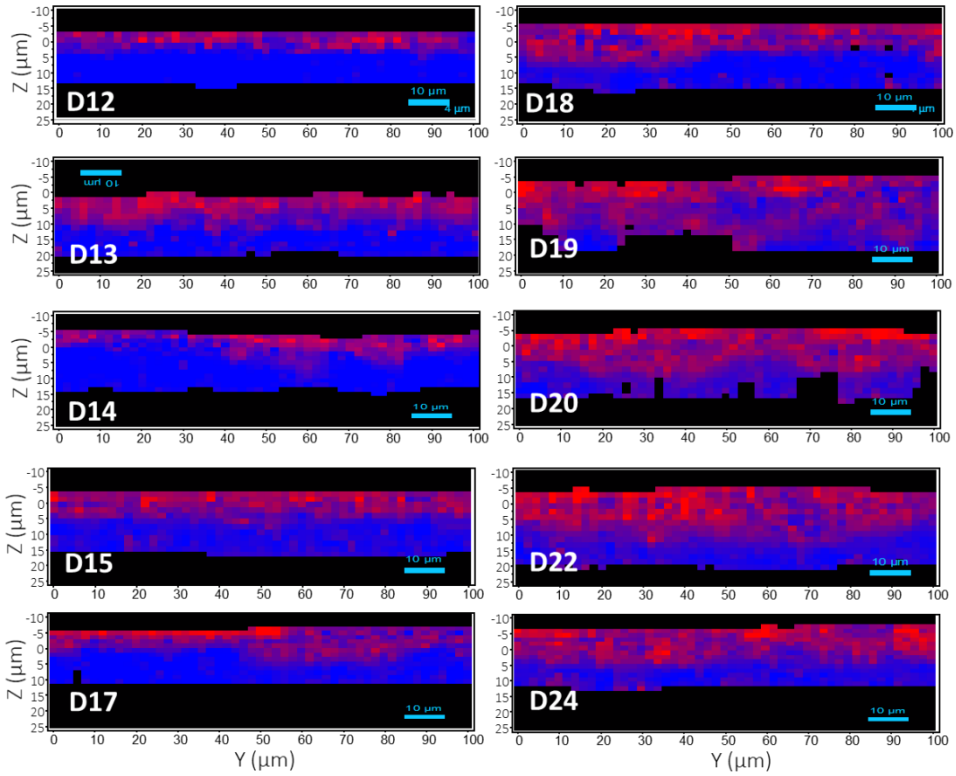

Figure 4 *Pseudo color maps obtained by CLS fitting. The evolution of the SC (Red color) compared to the granular layer (Blue color) during RHE maturation days. Raman spectra of RHE model at each maturation day were fitted with the reference spectra of human isolated SC and SG.*

The lipid conformational state

In this part, we aim to study first the evolution of the lipids' organization during the maturation of keratinocytes and then the relationship between the caffeine percutaneous penetration and the organization of the lipids in the epidermis. The ratio of ν_{asym} CH_2 (2882 cm^{-1})/ν_{sym} CH_2 (2852 cm^{-1}) was also calculated as shown in figure 5. This ratio is associated with the organizational order of lipids. The false color images were reconstructed based on the values of this ratio at each pixel of the image. Higher organizational order associated to a high ratio is represented in green to red while the lower order is colored in blue. For the first group, D12 and D14 showed lower values of organizational order. These results are in concordance with the data of caffeine penetration, revealing high permeability for these days. The plot of the organizational order showed a continuing rise increase in the *SC* lipid organization from D15 up to D24. It is worthy to notice the presence of higher number of red pixels D15 and D20 with a heterogeneous distribution in the *SC*. Compared to the observations on caffeine penetration (figure 2 and 3) these two days correspond to the transition days between the two groups.

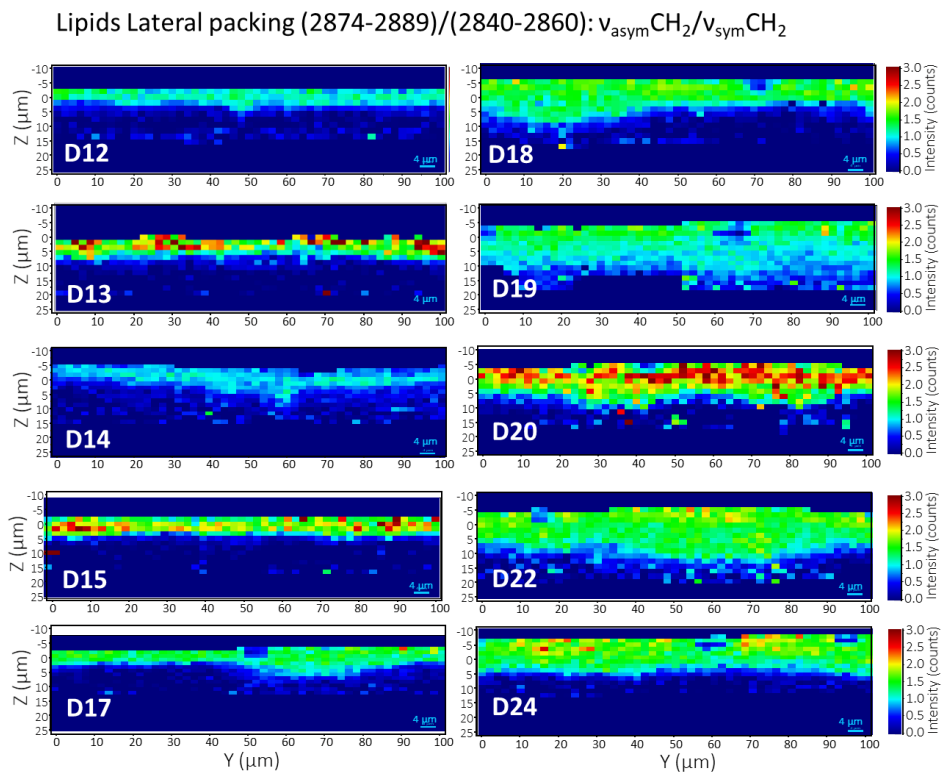

Figure 5 *Pseudo color maps representing the conformational state and lateral packing of lipids in the Stratum Corneum of RHE: $\nu_{asym}CH_2$ (2882 cm^{-1})/$\nu_{sym}CH_2$ (2852 cm^{-1}) ratio. High values are associated with higher trans content and a compact organization. High number of red pixels indicates a heterogeneous distribution in the SC.*

<u>The evolution of the lipid biomarkers during the differentiation process</u>

Ceramides, Glucosylceramides and Sphingomyelins classes are considered as biomarkers for lipid biosynthesis during the differentiation process. The analytical method used in this study was previously developed by our group [1] and was able to separate epidermis lipid classes in one single run. Figure 6 represents the chromatographic profile obtained for RHE models at D22 [1]. In this method, the lipid elution depends on the polar moieties (or "head group") of each lipid class. The Ceramide class is divided into different subclasses which differ in their structural micro heterogeneity, due to the number of hydroxylation, the number of unsaturation, the chain-length of amide-linked fatty acid and the isomers. Our analytical method is thus able to separate ceramide subclasses which are present in the form of several peaks between 18.3 and 30 min as shown in figure 6. As for Glucosylceramides and Sphingomyelins, all the lipids of each class were eluted in a one single chromatographic peak at 36.88 and 43.11 minutes of retention time respectively. This is due to the polarity of the glycosyl and phosphocholine groups, which is greater than the polarity differences induced by structural micro-heterogeneity [1]. Figure 7 presents the evolution of the 3 lipids biomarkers ceramides,

glucosylceramides and sphingomyelins respectively during the differentiation process. Results show that the amount of ceramides increased while the amounts of glucosylceramides and sphingomyelins decreased throughout the differentiation. Marked increases can be observed at D14 and D18: these increases occur 24 to 48 hours before we can see a noticeable decrease in the caffeine penetration profile and an important lipid organization.

The evolution of the ceramides' subclasses

Ceramides play a key role in the skin barrier function [18]. Ceramides with ultra-long chain (ULC) of fatty acids (≥ C26) such as esterified ceramides, are the major components of the barrier and of the extracellular multi-lamellar lipid layers of *SC* [19]. For this reason, the evolution of each ceramide subclass was carried out using NPLC/HR-MS^n and NPLC/Corona simultaneously[1]. The identification of each ceramide subclass in each chromatographic peak was determined previously [1] and the areas of the corresponding chromatographic peaks were measured. In general, all ceramides subclasses increased along the differentiation process (figure 8). Ceramides with retention time between 18.3-19.75 min (yellow line) regrouped subclasses with the most nonpolar ceramides such as ceramides with very long chain of fatty acid (ENH,ENT,EAP) [1], and also the new ceramide subclasses, a double esterified ceramides such as cer 1-O-E(EO)T, cer 1-O-E(EO)S and cer 1-O-E(EO)H [1]. Ceramide subclasses with retention time between 20-22.5 min (gray line) and 24.5-28 min (orange line) regrouped (EOS, EAH NS, Nds,) and (NP, Ads, AS, AP, EOH, NH) respectively and had a moderate polarity. Ceramides with a very polar head which have several hydroxyl groups such as (AH, NT) were detected at retention times between 29-30 min (blue line).

Interestingly, very marked variations can be observed at D14, D18 and D24.

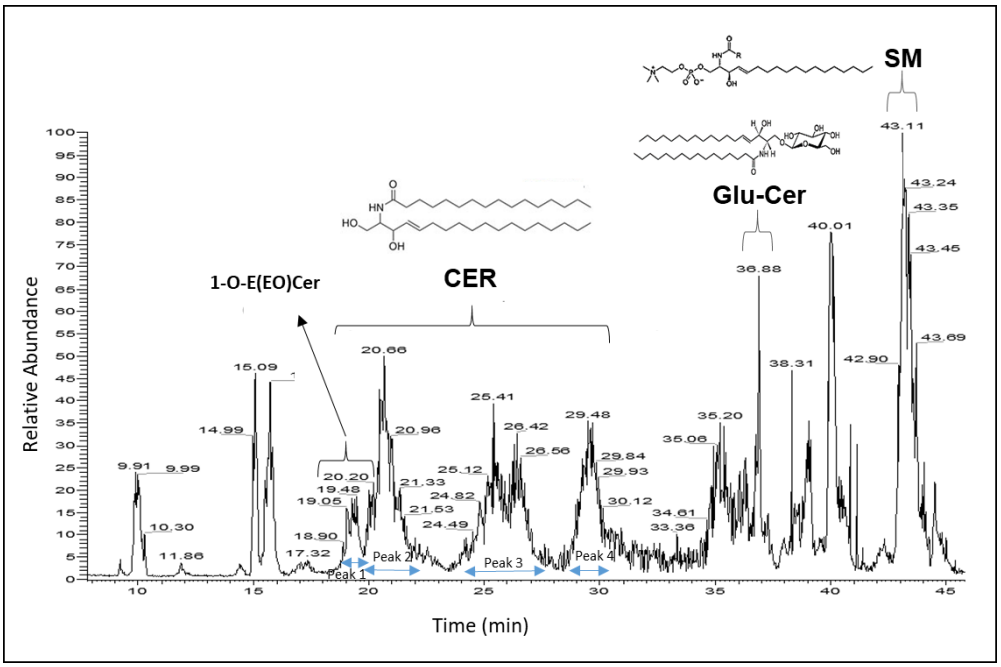

Figure 6 *NPLC/Corona chromatographic profile of three lipid biomarkers classes (Ceramides, Glucosylceramides and sphingomyelins) obtained for the RHE culture at D22. CER classes are divided into several subclasses and are presented in the form of several massive between 18.30-30 min [1].*

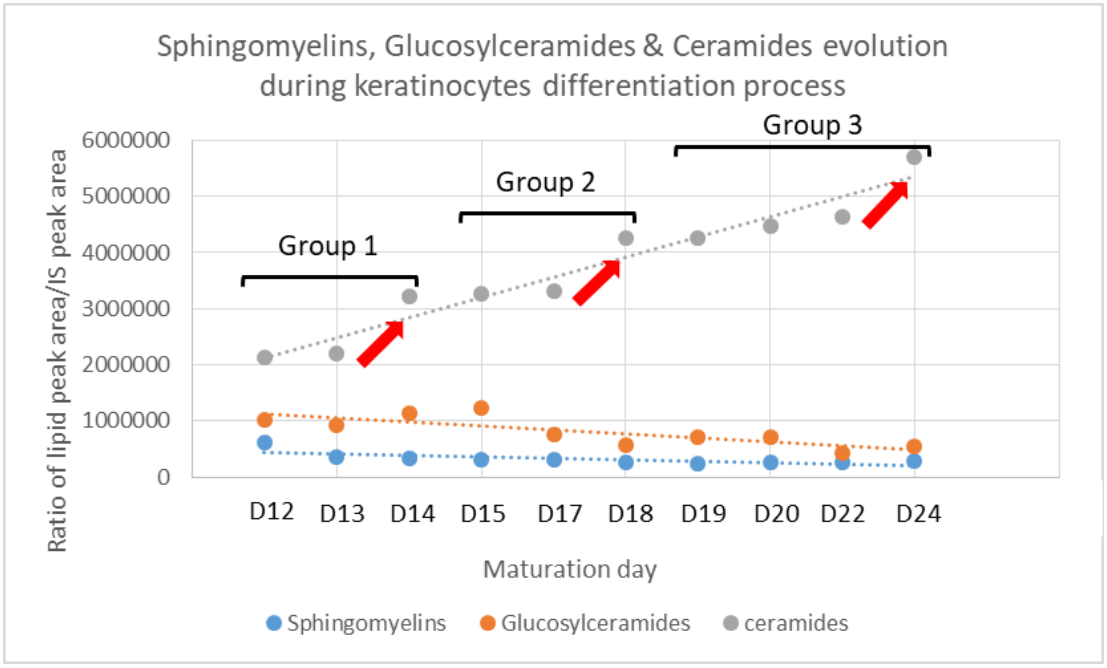

Figure 7 *Ceramides, Glucosylceramides and Sphingomyelins evolution during keratinocyte differentiation process. The total lipids of RHE samples were extracted and analyzed using NPLC/HR-MS^n and HPLC/Corona. The grey linear trendline presents the evolution of sum of ceramide peak areas divided by internal standard (IS) area. The orange linear trendline presents the evolution of glucosylceramide peak areas divided by internal standard area. The blue linear trendline presents the evolution of Sphingomyelin peak areas divided by internal standard area.*

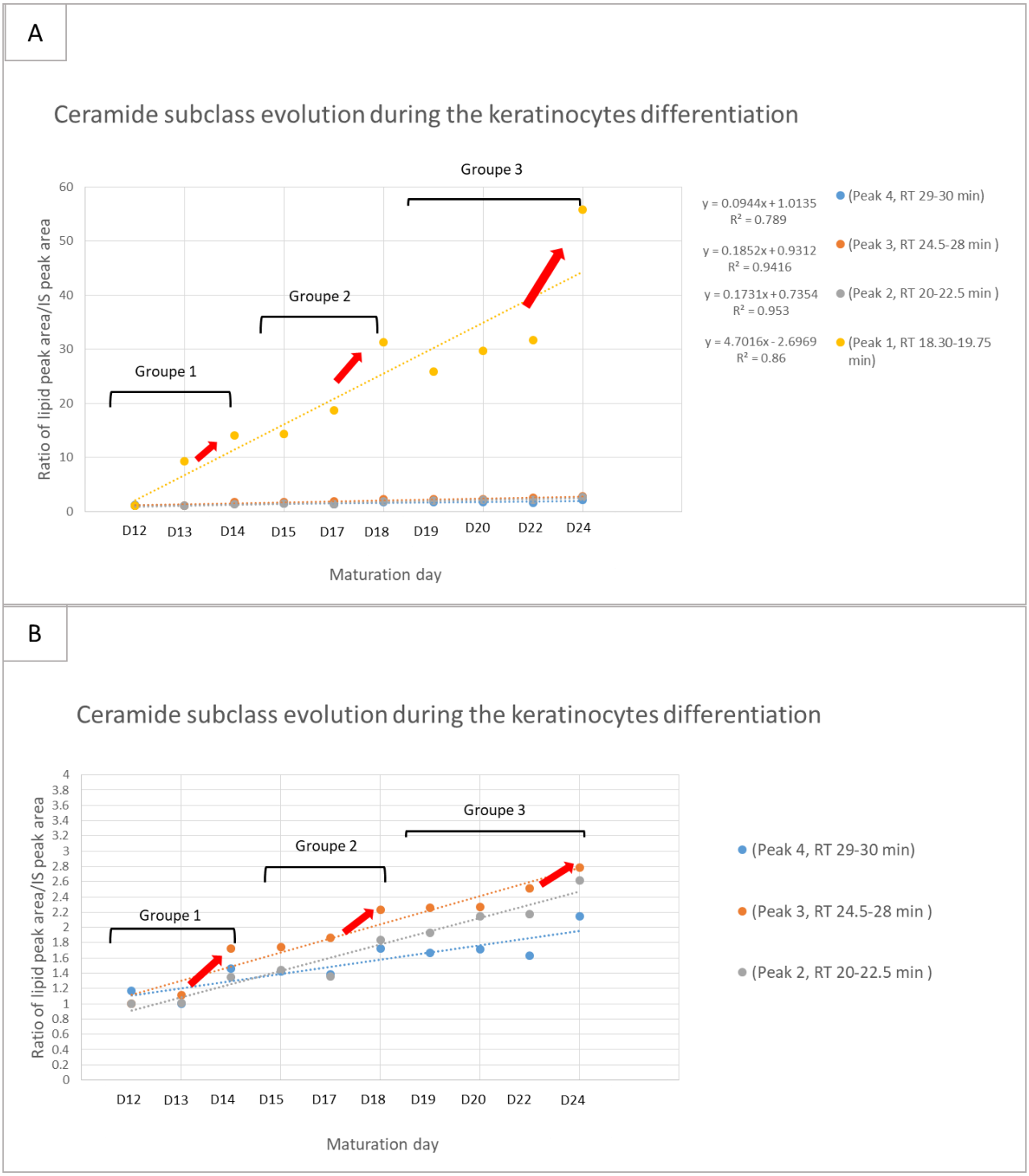

Figure 8 *The evolution of the ceramide subclasses during keratinocyte differentiation process. The total lipids of RHE samples were extracted and analyzed using NPLC/HR-MS^n and HPLC/Corona. The evolution of ceramide subclasses between retention times of 18.3 minutes and 30 minutes was followed. The yellow trendline present the evolution of nonpolar ceramide subclasses (esterified ceramide) which have a very long chain of fatty acid part (ENH,ENT,EAP and 1-O-E(EO)Cer)* ***(A).*** *The grey and orange trendline presents the evolution of ceramides with a moderate polarity (EOS,EAH,NS,NDS) and (NP, Ads, AS, AP,EOH, NS) respectively* ***(B).*** *The blue trendlines presents the evolution of the most polar ceramides (AH,NT)* ***(B).***

Discussion

In this work, the keratinocyte differentiation process was followed from D12 to D24. We used the multimodal approach described above because it has the advantage of offering different types of data that can converge and provide relevant and solid information to characterize the skin barrier functionality and to establish a link between the barrier function and the structure and the composition of the *SC*.

The barrier function of human skin resides in the *SC* [19]. In this study, the caffeine penetration study gives a first assessment of the skin barrier function.

The properties of the skin barrier depend on the *SC* lipids organization[3, 20]. Alteration in *SC* lipid organization can impair epidermal function and lead to skin diseases [19]. In this study, Raman spectroscopy provided us several information about the lipid organization, the epidermis thickness and the *SC* evolution.

The lipid composition also plays a key role in the skin barrier function[21]. Ceramides are the dominant lipid class (over 50%) of the total lipids species in the outermost epidermal layer. Then at the interface between the *SG* and *SC*, two ceramide precursors (sphingomyelins and glucosylceramides) are converted back to their ceramides species [22]. Thus, it is important to follow the ceramides precursors' evolution and to provide additional information about the stage of the keratinocytes' maturation. In this study, and for the first time, the evolution of keratinocytes' differentiation biomarkers (ceramides, glucosylceramides and sphingomyelins) was studied not only at the *SC* level but also at an earlier stage of the keratinocytes' differentiation.

However, skin diseases are correlated to lipid abnormality including modification in ceramide subclasses [23]. Thus, it is important to assess the evolution of ceramide subclasses during the differentiation process. This investigation was achieved using the NPLC/HR-MS^n.

It was observed that the caffeine penetration decreased during the RHE maturation. A clear evolution in the *Stratum Corneum* had been detected, with a better lipid organization at the later maturation days. Regarding the lipid composition, the ceramides level was increased throughout the differentiation, whereas in contrast, a decrease in the glucosylceramides and sphingomyelins levels was observed. In our study, we could distinguish 3 phases of maturation:

- <u>Maturation phase I:</u> between D 12 and D 14: results indicate that at this stage that the barrier function was not established yet. A high caffeine penetration throughout the RHE was observed with an important variation of values intra-group (figure 2). RHE was thinner (figure 3), the *SC* contribution in the RHE was the lowest (figure 4). In addition, there was a weak compact organization associated with a random behavior. During this phase, the total

ceramide amount was lower compared to the next phases. Inversely, the glucosylceramide and sphingomyelin levels were more abundant compared with the other maturation phases. The high value of these ceramides precursors is due to the high glycosylation and phosphorylation of ceramides into glucosylceramides, and sphingomyelins respectively,which occur before the *SC* and particularly with a high degree at the SG [18, 24]. For this reason, we were able to conclude that before D15, the *SC* was not fully formed.

- Maturation phase II: between D 15 and D 19: Caffeine penetration was less important compared with previous maturation phases but still not enough compared to the increase of the epidermis thickness (figure 3). These observations confirm that the barrier function is not only determined by RHE thickness, but rather by the organization of the intercellular lipids. In addition, the ceramide amount was increased. In contrast, glucosylceramides showed a high decrease after D15. Glucosylceramides are considered as precursors for the most *SC* ceramides; they convert back to the ceramides at the interface between the SG and *SC*. For this reason, their clear decrease after D15 is correlated with the high increase in ceramides. Unlike glucosylceramides, sphingomyelins are precursors for only some of the ceramides subclasses[25, 26]. Furthermore, sphingomyelins are present in high quantities at the SG cells membranes[26, 27]. This double sphingomyelin origin in keratinocytes may explain its less important decrease due to the ceramides biosynthesis compared to glucosylceramides. In conclusion, after D15, the *SC* forms a continuous layer, with good organization order, in the RHE model. As previously mentioned this observation is in concordance with data provided from Raman microspectroscopy suggesting a transition from SG to *SC*. In fact, at D15, in depth Raman imaging (figure 4) demonstrated higher red pixels heterogeneously distributed indicating a heterogeneous distribution in the *SC* and thus, D15 may be identified as a transition day between two phases of differentiation days. All of these data provided from the multimodal approach confirm that between D15-D19 the *Stratum Corneum* was formed and the barrier function was established.

- Maturation phase III: between D20 and D 24: the caffeine penetration decreased more and more. In addition, the RHE thickness and *SC* evolution were more important and the lipid organization was higher. Ceramides reached their maximum value, on the other hand glucosylceramides and sphingomyelins attained their lowest values. Similar to D15, D20 can be identified as a transition day between two phases. These results demonstrated that the multilayers of the *SC* continue to form during the last maturation days with good functionality of the skin barrier. A high value of

SC contribution in RHE Raman spectral signatures (supplementary data 2, table 1) was detected and a higher *trans* content which showed a better organized and more compact lipids.

It is worthy to take note of the presence of a shift of about 24h to 48h between the formation of the lipids and their organization. For example, an increase in the amount of ceramides was observed at D14, while an enhancement in the organization of lipids was detected at D15. Similarly, the same observation was obtained at D18-D19 for an enhancement of the organization at D20.

Furthermore, although the amount of each ceramide subclass increased throughout the differentiation, the relative increase is different from one subclass to another depending on the biosynthesis stage in the epidermis [25]. Thus, the increase of the nonpolar ceramides subclasses such as ceramides with very long chain (ENH, ENT, EAP, and 1-O-E (EO) Cer) (RT =18.3-19.75min) throughout differentiation days, was more important compared to the polar ceramides (RT 29-30 min) (figure 8). These nonpolar ceramide subclasses may generate at a late stage of the differentiation process and particularly at the interface between SG and *SC* [25]. Regarding their hydrophobicity, these subclasses play an important role in the barrier function. This may confirm the establishment of the RHE barrier function starting D15.

In fact, and thanks to our multimodal approach, we could conclude that for studies involving the barrier function of RHE models, it would be ideal to use these models from the 15th day of differentiation. However, studies related to cytotoxicity, irritation, corrosion could be applied before D15, since they are not related to the barrier function. By studying the last maturation days (D20-D24) we did not observe an alteration of the barrier function, but on the contrary, the *SC* continued its thickening and the lipids presented a better organization with a large quantity of ceramides. This maturation phase could be used when studying the impact of an active ingredient over a long duration of application.

In conclusion, this multimodal approach allows to fine select the maturation day of keratinocytes according to the type of the study that should be conducted.

Conclusion

The use of the reconstructed epidermis model has well evolved in order to better meet the needs of researchers. The choice of the maturation period varies according to the purpose of the study. In this work we presented a multimodal approach which has a very high capacity to offer complementary information, which is crucial to link the barrier function with the structure of the *SC*. Thus, the barrier function of the *Stratum Corneum* is not only determined by its

formation and its thickness but also by the composition and the structural organization of its intercellular lipids and the homogeneity of their formation. This approach allows the researchers to determine the period maturation which corresponds to their analysis goal.

Acknowledgements

The authors would like to thank the SILAB - Jean PAUFIQUE Corporate Foundation of the financial support for this work.

Compliance with ethical standards Conflict of interest

The authors declare that they have no conflict of interest.

References

1. A. Assi, J. Bakar, D. Libong, E. Sarkees, A. Solgadi, A. Baillet-Guffroy, R. Michael-Jubeli and A. Tfayli, *Analytical and bioanalytical chemistry*, 2019, DOI: 10.1007/s00216-019-02301-3.
2. M. Ponec, E. Boelsma, A. Weerheim, A. Mulder, J. Bouwstra and M. Mommaas, *International journal of pharmaceutics*, 2000, **203**, 211-225.
3. M. Ponec, E. Boelsma, S. Gibbs and M. Mommaas, *Skin pharmacology and applied skin physiology*, 2002, **15 Suppl 1**, 4-17.
4. M. Ponec, S. Gibbs, G. Pilgram, E. Boelsma, H. Koerten, J. Bouwstra and M. Mommaas, *Skin pharmacology and applied skin physiology*, 2001, **14 Suppl 1**, 63-71.
5. J. A. Bouwstra, G. S. Gooris, A. Weerheim, J. Kempenaar and M. Ponec, *J Lipid Res*, 1995, **36**, 496-504.
6. M. Ponec, A. Weerheim, J. Kempenaar, A. Mulder, G. S. Gooris, J. Bouwstra and A. M. Mommaas, *J Invest Dermatol*, 1997, **109**, 348-355.
7. A. Tfayli, F. Bonnier, Z. Farhane, D. Libong, H. J. Byrne and A. Baillet-Guffroy, *Exp Dermatol*, 2014, **23**, 441-443.
8. L. J. Lowenau, C. Zoschke, R. Brodwolf, P. Volz, C. Hausmann, S. Wattanapitayakul, A. Boreham, U. Alexiev and M. Schafer-Korting, *European journal of pharmaceutics and biopharmaceutics : official journal of Arbeitsgemeinschaft fur Pharmazeutische Verfahrenstechnik e.V*, 2017, **116**, 149-154.
9. G. Potard, C. Laugel, A. Baillet, H. Schaefer and J. P. Marty, *International journal of pharmaceutics*, 1999, **189**, 249-260.
10. F. Netzlaff, M. Kaca, U. Bock, E. Haltner-Ukomadu, P. Meiers, C. M. Lehr and U. F. Schaefer, *European journal of pharmaceutics and biopharmaceutics : official journal of Arbeitsgemeinschaft fur Pharmazeutische Verfahrenstechnik e.V*, 2007, **66**, 127-134.
11. R. Darlenski, S. Sassning, N. Tsankov and J. W. Fluhr, *European journal of pharmaceutics and biopharmaceutics : official journal of Arbeitsgemeinschaft fur Pharmazeutische Verfahrenstechnik e.V*, 2009, **72**, 295-303.

12. S. Tfaili, C. Gobinet, G. Josse, J. F. Angiboust, A. Baillet, M. Manfait and O. Piot, *Analytical and bioanalytical chemistry*, 2013, **405**, 1325-1332.
13. L. Verzeaux, R. Vyumvuhore, D. Boudier, M. Le Guillou, S. Bordes, M. Essendoubi, M. Manfait and B. Closs, *Exp Dermatol*, 2017, **27**, 403-408.
14. C. A. Brohem, L. B. Cardeal, M. Tiago, M. S. Soengas, S. B. Barros and S. S. Maria-Engler, *Pigment cell & melanoma research*, 2011, **24**, 35-50.
15. E. G. Bligh and W. J. Dyer, *Can J Biochem Phys*, 1959, **37**, 911-917.
16. A. Tfayli, O. Piot and M. Manfait, *Journal of biophotonics*, 2008, **1**, 140-153.
17. A. Tfayli, E. Guillard, M. Manfait and A. Baillet-Guffroy, *Analytical and bioanalytical chemistry*, 2010, **397**, 1281-1296.
18. M. H. Meckfessel and S. Brandt, *Journal of the American Academy of Dermatology*, 2014, **71**, 177-184.
19. B. Breiden and K. Sandhoff, *Biochim Biophys Acta*, 2014, **1841**, 441-452.
20. J. van Smeden and J. A. Bouwstra, *Current problems in dermatology*, 2016, **49**, 8-26.
21. M. Danso, W. Boiten, V. van Drongelen, K. Gmelig Meijling, G. Gooris, A. El Ghalbzouri, S. Absalah, R. Vreeken, S. Kezic, J. van Smeden, S. Lavrijsen and J. Bouwstra, *J Dermatol Sci*, 2017, **88**, 57-66.
22. Y. Mizutani, S. Mitsutake, K. Tsuji, A. Kihara and Y. Igarashi, *Biochimie*, 2009, **91**, 784-790.
23. F. F. Sahle, T. Gebre-Mariam, B. Dobner, J. Wohlrab and R. H. Neubert, *Skin pharmacology and physiology*, 2015, **28**, 42-55.
24. P. M. Elias, *J Invest Dermatol*, 1983, **80**, 44s-49s.
25. M. Rabionet, K. Gorgas and R. Sandhoff, *Bba-Mol Cell Biol L*, 2014, **1841**, 422-434.
26. Y. Uchida, M. Hara, H. Nishio, E. Sidransky, S. Inoue, F. Otsuka, A. Suzuki, P. M. Elias, W. M. Holleran and S. Hamanaka, *J Lipid Res*, 2000, **41**, 2071-2082.
27. B. Ramstedt and J. P. Slotte, *Febs Lett*, 2002, **531**, 33-37.